

Relativistic Collapse of Rotating Supermassive Stars to Supermassive Black Holes

Stuart L. Shapiro

University of Illinois at Urbana-Champaign

Abstract

There is compelling evidence that supermassive black holes (SMBHs) exist. Yet the origin of these objects, or their seeds, is still unknown. We are performing general relativistic simulations of gravitational collapse to black holes in different scenarios to help reveal how SMBH seeds might arise in the universe. SMBHs with $\sim 10^9 M_\odot$ must have formed by $z > 6$, or within 10^9 yrs after the Big Bang, to power quasars. It may be difficult for gas accretion to build up such a SMBH by this time unless the initial seed black hole already has a substantial mass. One plausible progenitor of a massive seed black hole is a supermassive star (SMS). We have followed the collapse of a SMS to a SMBH by means of 3D hydrodynamic simulations in post-Newtonian gravity and axisymmetric simulations in full general relativity. The initial SMS of arbitrary mass M in these simulations rotates uniformly at the mass-shedding limit and is marginally unstable to radial collapse. The final black hole mass and spin are determined to be $M_h/M \approx 0.9$ and $J_h/M_h^2 \approx 0.75$. The remaining mass goes into a disk of mass $M_{\text{disk}}/M \approx 0.1$. This disk arises even though the total spin of the progenitor star, $J/M^2 = 0.97$, is safely below the Kerr limit. The collapse generates a mild burst of gravitational radiation. Nonaxisymmetric bars or one-armed spirals may arise during the quasi-stationary evolution of a SMS, during its collapse, or in the ambient disk about the hole, and are potential sources of quasi-periodic waves, detectable by LISA.

Introduction

There is substantial evidence that supermassive black holes (SMBHs) of mass $\sim 10^6 - 10^{10} M_\odot$ exist and are the engines that power active galactic nuclei (AGNs) and quasars [30, 31, 32, 26]. There is also ample evidence that SMBHs reside at the centers of many, and perhaps most, galaxies [33, 23], including the Milky Way [19, 20, 37].

Since quasars have been discovered out to redshift $z \gtrsim 6$ [13, 14], the first SMBHs must have formed by $z_{\text{BH}} \gtrsim 6$, or within $t_{\text{BH}} \lesssim 10^9$ yrs after the Big Bang. However, the cosmological origin of SMBHs is not known. This issue remains one of the crucial, unresolved aspects of structure formation in the early universe. Gravitationally, black holes are strong-field objects whose properties are governed by Einstein's theory of relativistic gravitation — general relativity. General relativistic simulations of gravitational collapse to black holes therefore may help reveal how, when and where SMBHs, or their seeds, form in the universe. Simulating plausible paths by which the very first seed black holes may have arisen comprises a timely computational challenge (see Fig. 1). It is an area in which the tools of numerical relativity may be exploited to address a fundamental question in cosmology. Performing such simulations may also help identify plausible astrophysical scenarios and sites for promising gravitational wave sources involving black holes.

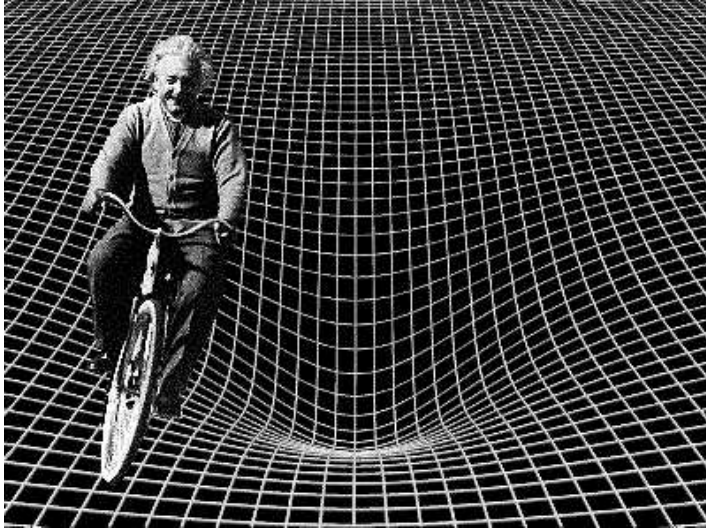


Figure 1: The formation of a black hole is a strong-field gravitational phenomenon in curved spacetime that requires Einstein’s equations of general relativity for a description and, in non-trivial cases, numerical simulations for a solution.

We are actively developing new algorithms and new computer codes to solve Einstein’s field equations of general relativity, coupled to the equations of relativistic hydrodynamics, in three spatial dimensions plus time (3+1). As our codes have come online, we have applied them to explore different astrophysical scenarios involving strong gravitational fields and the generation of gravitational waves. These have included the inspiral and coalescence of binary neutron stars and binary black holes, the growth of instabilities in rotating stars, the nonlinear evolution of unstable stars, and the collapse and collision of rotating stars and rotating clusters of collisionless matter, to name a few. [For recent reviews of simulations of compact binary stars and references, see [29] and [3]]. We have also performed a wide range of simulations in recent years to study alternative scenarios leading to the formation of supermassive black holes, or their seeds. [For a review of these calculations and references, see [38]] Here we will focus on one specific scenario, namely, the collapse of a rotating, supermassive star (SMS) to a supermassive black hole.

The Onset of Dynamical Instability

The formation of SMBHs through the growth of black hole seeds by gas accretion is supported by the consistency between the total energy density in QSO light and the SMBH mass density in local galaxies, adopting a reasonable accretion rest-mass-to-energy conversion efficiency [46, 49]. But SMBHs must be present by $z_{\text{BH}} \gtrsim 6$ to power quasars. It has been argued [21] that if they grew by accretion from smaller seeds, substantial seeds of mass $\gtrsim 10^5 M_{\odot}$ must already be present at $z \approx 9$ to have had sufficient time to build up to a typical quasar black hole mass of $\sim 10^9 M_{\odot}$. A likely progenitor is a very massive object (e.g., an SMS) supported by radiation pressure.

SMSs ($10^3 \lesssim M/M_{\odot} \lesssim 10^{13}$) may form when contracting or colliding primordial gas builds up sufficient radiation pressure to inhibit fragmentation and prevent star formation (see, e.g., [6]). SMSs supported by radiation pressure will evolve in a quasi-stationary manner to the point of

onset of dynamical collapse due to general relativity [9, 10, 15] Unstable SMSs with $M \gtrsim 10^5 M_\odot$ and metallicity $Z \lesssim 0.005$ do not disrupt due to thermonuclear explosions during collapse [18]. In fact, recent Newtonian simulations suggest that evolved zero-metallicity (Pop III) stars $\gtrsim 300 M_\odot$ do not disrupt but collapse with negligible mass loss [17]. This finding could be important since the first generation of stars may form in the range $10^2 - 10^3 M_\odot$ [5, 1]. A combination of turbulent viscosity and magnetic fields likely will keep a spinning SMS in uniform rotation ([4, 47, 50, 39]; but see [27] and the final section below for an alternative). As they cool and contract, uniformly rotating SMSs reach the maximally rotating *mass-shedding limit* and subsequently evolve in a quasi-stationary manner along a mass-shedding sequence until reaching the instability point. At mass-shedding, the matter at the equator moves in a circular geodesic with a velocity equal to the local Kepler velocity [2].

It is straightforward to understand the radial instability induced by general relativity in a SMS by using an energy variational principle [50, 42]. Let $E = E(\rho_c)$ be the total energy of a momentarily static, spherical fluid configuration characterized by central mass density ρ_c . The condition that $E(\rho_c)$ be an extremum for variations that keep the total rest mass and specific entropy distribution fixed is equivalent to the condition of hydrostatic equilibrium and establishes the relation between the equilibrium mass and central density:

$$\frac{\partial E}{\partial \rho_c} = 0 \implies M_{\text{eq}} = M_{\text{eq}}(\rho_c) \quad (\text{equilibrium}). \quad (1)$$

The condition that the second variation of $E(\rho_c)$ be zero is the criterion for the onset of dynamical instability. This criterion shows that the turning point on a curve of equilibrium mass vs. central density marks the transition from stability to instability:

$$\frac{\partial^2 E}{\partial \rho_c^2} = 0 \iff \frac{\partial M_{\text{eq}}}{\partial \rho_c} = 0 \quad (\text{onset of instability}). \quad (2)$$

Consider the simplest case of a spherical Newtonian SMS supported solely by radiation pressure and endowed with zero rotation. This is an $n = 3$, ($\Gamma = 1 + 1/n = 4/3$) polytrope, with pressure

$$P = P_{\text{rad}} = \frac{1}{3}aT^4 = K\rho^{\frac{4}{3}}, \quad (3)$$

where $K = K(s_{\text{rad}})$ is a constant determined by the value of the (constant) specific entropy $s_{\text{rad}} = \frac{4}{3}aT^3/n$ in the star. Here T is the temperature, n is the baryon number density, and a is the radiation constant. Consider a sequence of configurations with the same specific entropy but different values of central density. The total energy of each configuration is

$$E(\rho_c) = U_{\text{rad}} + W, \quad (4)$$

where U_{rad} is the total internal radiation energy and W is the gravitational potential energy. Applying the equilibrium condition (1) to this functional yields $M_{\text{eq}} = M_{\text{eq}}(s_{\text{rad}})$, i.e. the equilibrium mass depends only on the specific entropy and is independent of central density (see Fig. 2a). Applying the stability condition (2) then shows that all equilibrium models along this sequence are marginally stable to collapse.

Now let us account for the effects of general relativity. If we include the small (de-stabilizing) Post-Newtonian (PN) correction to the gravitational field, we must also include a comparable (stabilizing) correction to the equation of state arising from thermal gas pressure:

$$P = P_{\text{rad}} + P_{\text{gas}} = \frac{1}{3}aT^4 + 2nkT, \quad (5)$$

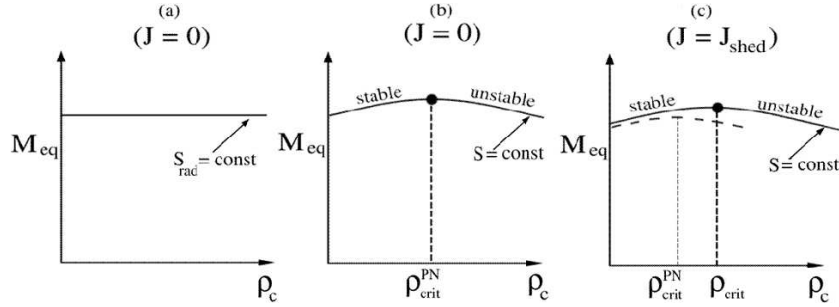


Figure 2: A sketch of mass versus central density along an equilibrium sequence of SMSs of fixed entropy. Panel (a) shows nonrotating, spherical Newtonian models supported by pure radiation pressure; (b) shows nonrotating, spherical PN models supported by radiation pressure plus thermal gas pressure; (c) shows rotating PPN models spinning at the mass-shedding limit.

where we have taken the gas to be pure ionized hydrogen. Note that $P_{\text{gas}}/P_{\text{rad}} = 8/(s_{\text{rad}}/k) \ll 1$. The energy functional of a star now becomes

$$E(\rho_c) = U_{\text{rad}} + W + \Delta U_{\text{gas}} + \Delta W_{\text{PN}}, \quad (6)$$

where ΔU_{gas} is the internal energy perturbation due to thermal gas energy and ΔW_{PN} is the PN perturbation to the gravitational potential energy. Applying the equilibrium condition (1) now yields $M_{\text{eq}} \approx M_{\text{eq}}^{\text{Newt}}$ times a slowly varying function of ρ_c (see Fig. 2b). The turning point on the equilibrium curve marks the onset of radial instability; the marginally stable critical configuration is characterized by

$$\begin{aligned} \rho_{c,\text{crit}} &= 2 \times 10^{-3} M_6^{-7/2} \text{ gm cm}^{-3}, \\ T_{c,\text{crit}} &= (3 \times 10^7) M_6^{-1} \text{ K}, \\ (R/M)_{\text{crit}} &= 1.6 \times 10^3 M_6^{1/2}, \end{aligned} \quad (7)$$

where M_6 denotes the mass in units of $10^6 M_\odot$. (Here and throughout we adopt gravitational units and set $G = 1 = c$.)

Finally, let us consider a uniformly rotating SMS spinning at the mass-shedding limit [2]. A centrally condensed object like an $n = 3$ polytrope can only support a small amount of rotation before matter flies off at the equator. At the mass-shedding limit, the ratio of rotational kinetic to gravitational potential energy is only $T/|W| = 0.899 \times 10^{-2} \ll 1$. Most of the mass resides in a nearly spherical interior core, while the low-mass (Roche) envelope bulges out in the equator: $R_{\text{eq}}/R_{\text{pole}} = 3/2$. When we include the contribution of rotational kinetic energy to the energy functional, we must now also include the effects of relativistic gravity to Post-Post-Newtonian (i.e. PPN) order, since both T and ΔW_{PN} scale with ρ_c to the same power. The energy functional becomes

$$E(\rho_c) = U_{\text{rad}} + W + \Delta U_{\text{gas}} + \Delta W_{\text{PN}} + \Delta W_{\text{PPN}} + T \quad (8)$$

Applying the equilibrium condition (1), holding M , angular momentum J and s fixed, now yields $M_{\text{eq}} \approx M_{\text{eq}}^{\text{Newt}}$ times a slowly varying function of ρ_c (see Fig. 2c). If we restrict our attention to rapidly rotating stars with $M > 10^5 M_\odot$ (the typical size of the seed black holes adopted in some recent galaxy merger simulations; see, e.g., [22]) the influence of thermal gas pressure is unimportant in determining the critical point of instability. The turning point on the equilibrium

curve then shifts to higher density and compaction than the critical values for nonrotating stars, reflecting the stabilizing role of rotation:

$$\begin{aligned}
\rho_{c,\text{crit}} &= 0.9 \times 10^{-1} M_6^{-2} \text{ gm cm}^{-3}, \\
T_{c,\text{crit}} &= (9 \times 10^7) M_6^{-1/2} \text{ K}, \\
(R_{\text{pole}}/M)_{\text{crit}} &= 427, \\
(J/M^2)_{\text{crit}} &= 0.97.
\end{aligned}
\tag{9}$$

The actual values quoted above for the critical configuration were determined by a careful numerical integration of the general relativistic equilibrium equations for rotating stars [2]; they are in close agreement with those determined analytically by the variational treatment. The numbers found for the nondimensional critical compaction and angular momentum are quite interesting. First, they are universal ratios that are independent of the mass of the SMS. This means that a single relativistic simulation will suffice to track the collapse of a marginally unstable, maximally rotating SMS of *arbitrary* mass. Second, the large value of the critical radius shows that a marginally unstable configuration is nearly Newtonian at the onset of collapse. Third, the fact that the angular momentum parameter of the critical configuration J/M^2 is below unity suggests that, in principle, the entire mass and angular momentum of the configuration could collapse to a rotating black hole in vacuum without violating the Kerr limit for black hole spin (but see the next section below!).

The Outcome of Collapse

There are several plausible outcomes that one might envision *a priori* for the dynamical collapse of a uniformly rotating SMS once it reaches the marginally unstable critical point identified above. It could collapse to a clumpy, nearly axisymmetric disk, similar to the one arising in the Newtonian SPH simulations for the isothermal ($\Gamma = 1$) implosion of an initially homogeneous, uniformly rotating, low-entropy cloud [25]. Alternatively, the disk might develop a large-scale, nonaxisymmetric bar. After all, the onset of a dynamically unstable bar mode in a spinning equilibrium star occurs when the ratio $T/|W| \approx 0.27$ (see, e.g., [11] and [24] for Newtonian treatments and [35] and [43] for simulations in general relativity). Since $T/|W|$ is 0.899×10^{-2} at the onset of collapse and scales roughly as R^{-1} during collapse, assuming conservation of mass and angular momentum, this ratio climbs above the dynamical bar instability threshold when the SMS collapses to $R/M \approx 20$, well before the horizon is reached. The growth of a bar might begin at this point. Indeed, a weak bar forms in simulations of rotating supernova core collapse [28, 7], but in supernova the equation of state stiffens ($\Gamma > 4/3$) at the end of the collapse, triggering a bounce and thereby allowing more time for the bar to develop. A rapidly rotating unstable SMS might not form a disk at all, but instead collapse entirely to a Kerr black hole; not surprisingly, a nonrotating spherical SMS has been shown to collapse to a Schwarzschild black hole [41]. Alternatively, the unstable rotating SMS might collapse to a rotating black hole *and* an ambient disk.

Recently we have performed two simulations that together resolve the fate of a marginally unstable, maximally rotating SMS of arbitrary mass M . In [36] we followed the collapse in full $3D$, but assumed PN theory. We tracked the implosion up to the point at which the central spacetime metric begins to deviate appreciably from flat space at the stellar center. We found that the massive core collapses homologously during the Newtonian epoch of collapse, and that axisymmetry is preserved up to the termination of the integrations. This calculation motivated us [45] to follow the collapse in full general relativity by assuming axisymmetry from the beginning

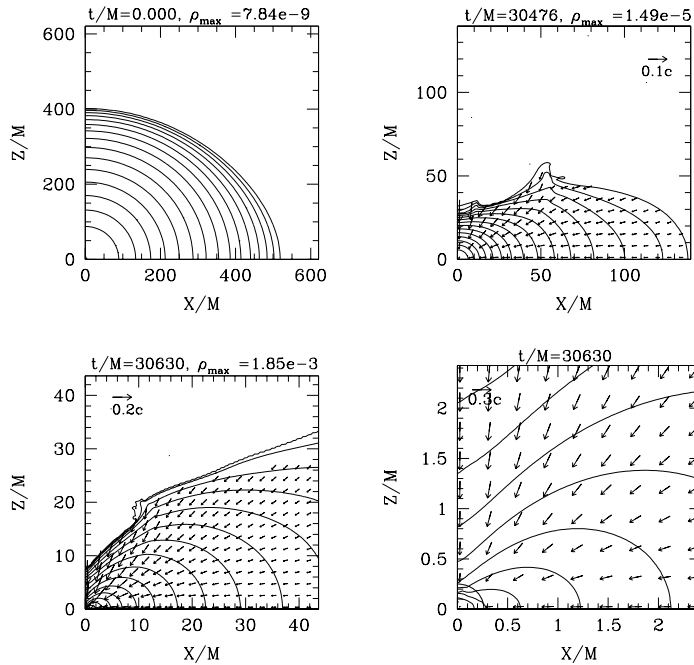


Figure 3: Snapshots of density and velocity profiles during the implosion of a marginally unstable SMS of arbitrary mass M rotating uniformly at break-up speed at $t = 0$. The contours are drawn for $\rho/\rho_{\max} = 10^{-0.4j}$ ($j = 0 - 15$), where ρ_{\max} denotes the maximum density at each time. The fourth figure is the magnification of the third one in the central region: the thick solid curve at $r \approx 0.3M$ denotes the location of the apparent horizon of the emerging SMBH. (From Shibata & Shapiro [45])

to maximize spatial resolution (see Fig. 3). We found that the final object is a Kerr-like black hole surrounded by a disk of orbiting gaseous debris. The final black hole mass and spin were determined to be $M_h/M \approx 0.9$ and $J_h/M_h^2 \approx 0.75$. The remaining mass goes into the disk of mass $M_{\text{disk}}/M \approx 0.1$. A disk forms even though the total spin of the progenitor star is safely below the Kerr limit. This outcome results from the fact that the dense inner core collapses homologously to form a central black hole, while the diffuse outer envelope avoids capture because of its high angular momentum. Specifically, in the outermost shells, the angular momentum per unit mass j , which is strictly conserved on cylinders, exceeds j_{ISCO} , the specific angular momentum at the innermost stable circular orbit about the final hole. This fact suggests how the final black hole and disk parameters can be calculated *analytically* from the initial SMS density and angular momentum distribution [40]. The result applies to the collapse of *any* marginally unstable $n = 3$ polytrope at mass-shedding. Maximally rotating stars which are characterized by stiffer equations of state and smaller n (higher Γ) do not form disks, typically, since they are more compact and less centrally condensed at the onset of collapse [44].

The above calculations show that a SMBH formed from the collapse of a maximally rotating SMS is always born with a “ready-made” accretion disk. This disk might provide a convenient source of fuel to power the central engine. The calculations also show that the SMBH will be born rapidly rotating. This fact is intriguing in light of suggestions that observed SMBHs rotate

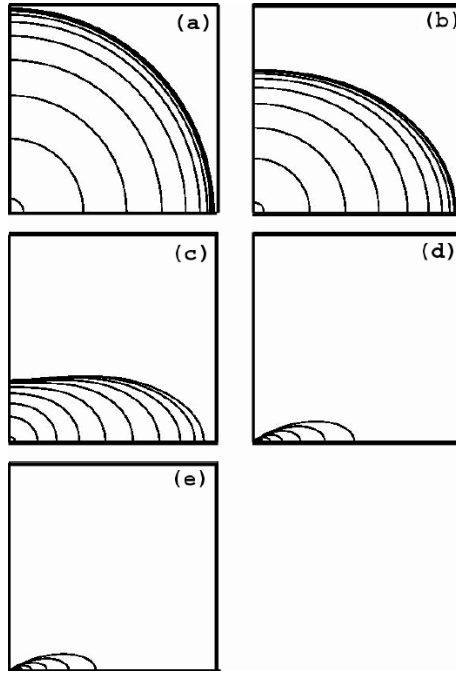


Figure 4: Quasi-stationary evolution snapshots of a SMS that cools and contracts in the absence of any viscosity or magnetic fields from a nearly spherical initial state that is in very slow, uniform rotation. The maximum density is normalized to unity; the highest density contour level is 0.9 and subsequent levels range from 10^{-1} to 10^{-10} and are separated by a decade. The final configuration has reached the mass-shedding limit and is toroidal and differentially rotating, with $T/|W| \approx 0.27$ and $\Omega_{\text{pole}}/\Omega_{\text{eq}} \approx 2.5 \times 10^3$. (From New & Shapiro [27])

rapidly (e.g., [48, 12]).

The implosion will result in a *burst* of gravitational waves. Current relativistic collapse calculations for this problem break down soon after the apparent horizon of the hole approaches its asymptotic size. Moreover, the need to resolve the centrally condensed inner core precludes extending the numerical grid very far out into the wave zone. These two restrictions prevent a reliable determination of the complete burst waveform at present. Crude estimates can be generated for the frequency and amplitude based on the quadrupole formula, and the results suggest that they are well within the range of detectability for LISA for a reasonable spectrum of masses. More interesting, perhaps, is the possible generation of *quasi-periodic* gravitational waves from nonaxisymmetric instabilities that might arise in the ambient disk; the characteristics of these waves are likely to be comparable those discussed in the next section and in Eqn. (10) below.

An Alternative Scenario

The previous analysis assumes that a combination of turbulent viscosity and magnetic fields combine to keep a spinning SMS rotating *uniformly* prior to the onset of collapse. While this is the most likely possibility [4, 47, 50, 39], New and Shapiro [27] have discussed an alternative. In the absence of viscosity or magnetic fields, an evolving SMS will conserve angular momentum on

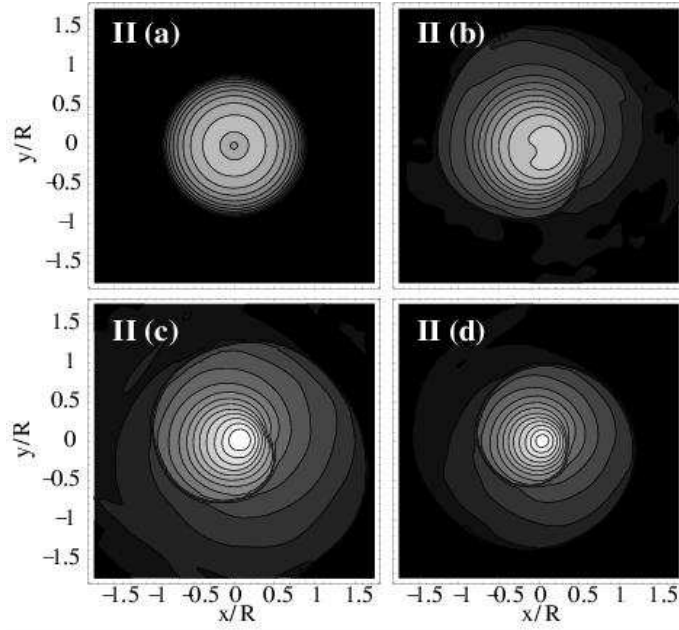


Figure 5: Snapshots of density contours in the equatorial plan of differentially rotating Newtonian toroids of different polytropic indicies, n . All of the stars are constructed from the same differential rotation law with $\Omega_{\text{pole}}/\Omega_{\text{eq}} \approx 26$ and $T/|W| \approx 0.14$ at $t = 0$. The snapshots are taken after the stars have evolved for many central rotation periods, P_c . Stars with higher n exhibit a one-armed spiral $m=1$ instability. The panels show results for $(n, t/P_c) = (a)(2, 37); (b)(2.5, 24); (c)(3, 17);$ and $(d)(3.33, 19)$. The contour lines denote densities $\rho/\rho_c = 10^{-(16-i)d}$ ($i = 1, \dots, 15$). (From Saijo, Baumgarte & Shapiro [34])

cylinders as it cools and contracts in a quasi-stationary manner. So even if it is rotating uniformly at formation, it will evolve to a state of *differential* rotation. Our evolution calculations indicate that an axisymmetric configuration that is slowly rotating uniformly and nearly spherical at birth ($T/|W| \ll 1$) will evolve to a differentially rotating toroid (see Fig. 4). Prior to encountering any relativistic radial instability, the star reaches the mass-shedding limit, at which point $T/|W| \approx 0.27$ and differential rotation is extreme, $\Omega_{\text{pole}}/\Omega_{\text{eq}} \approx 2.5 \times 10^3$.

Toroidal configurations which have high values of $T/|W|$ and substantial differential rotation and central mass concentration are subject to nonaxisymmetric dynamical instabilities, especially the one-armed spiral $m = 1$ instability [8, 34]. Softer equations of state with higher polytropic indicies are very susceptible to this instability (see Fig. 5), so this mode is likely to be triggered in a rotating SMS should it evolve with low viscosity and magnetic field. Such a mode typically induces a secondary $m=2$ bar mode of smaller amplitude, and the bar mode can excite quasi-periodic gravitational waves (see Fig. 6). Typical wave amplitudes and wave frequencies for a source at a distance r are given by

$$\begin{aligned}
 h &\sim 10^{-16}(T/|W|)(M/R)M_6 r_{\text{GPC}}^{-1} \sim 10^{-20}M_6 r_{\text{GPC}}^{-1}, \\
 f_{\text{GW}} &\sim 10^{-1}(T/|W|)^{1/2}(M/R)^{3/2}M_6^{-1}\text{Hz} \sim 10^{-4}M_6^{-1}\text{Hz}.
 \end{aligned}
 \tag{10}$$

where we have set $T/|W| \sim 0.27$ and $R/M \sim 10^3$ in evaluating the above quantities. These values also apply to waves generated by bar modes that may arise in a similar fashion in the ambient

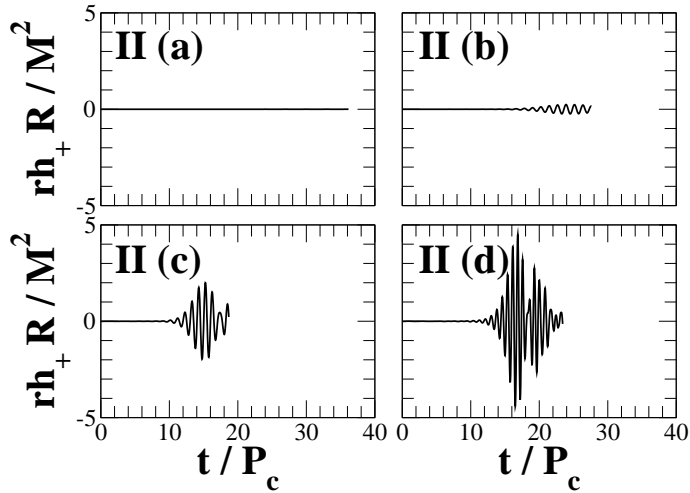


Figure 6: Gravitational radiation waveforms as seen by a distant observer on the rotation axis for the configurations shown in Fig. 5. The radius r is the distance to the source and the ratio M/R is the (arbitrary) compaction of the initial configuration. (From Saijo, Baumgarte & Shapiro [34])

disk surrounding the SMS black hole that forms from the collapse of a relativistically unstable, uniformly rotating SMS (see discussion above). Both the amplitudes and frequencies put these waves well within the detectable range for LISA for a realistic distribution of masses. Future simulations that we are planning will explore this possibility in greater detail, and help resolve which scenario best describes the final fate of a rotating SMS.

acknowledgments

This work was supported in part by NSF Grants PHY-0090310 and PHY-0205155 and NASA Grant NAG5-10781 at the University of Illinois at Urbana-Champaign.

References

- [1] Abel, T., Bryan, G. L., & Norman, M. L. 2000, *ApJ*, 540, 39
- [2] Baumgarte, T. W., & Shapiro, S. L. 1999, *ApJ*, 526, 941
- [3] Baumgarte, T. W., & Shapiro, S. L. 2003, *Phys. Reports*, 376/2, 41
- [4] Bisnovatyi-Kogan, G. S., Zel'dovich, Ya. B., & Novikov, I. D. 1967, *Soviet Astron.*, 11, 419
- [5] Bromm, V., Coppi, P. S., & Larson, R. B. 1999, *ApJ*, 527, L5
- [6] Bromm, V., & Loeb, A. 2003, *ApJ*, in press (astro-ph/0212400)
- [7] Brown, J. D. 2001, in *Astrophysical Sources for Ground-based Gravitational Wave Detectors*, ed. J. M. Centrella (New York: AIP), 234
- [8] Centrella, J. M., New, K. C. B., Lowe, L. L. & Brown, J. D. 2001, *ApJ*, 550, L193

- [9] Chandrasekhar, S. 1964a, *Phys. Rev. Lett.*, 12, 114, 437E
- [10] Chandrasekhar, S. 1964b, *ApJ*, 140, 417
- [11] Chandrasekhar, S. 1969, *Ellipsoidal Figures of Equilibrium* (New Haven: Yale Univ. Press)
- [12] Elvis, M., Risaliti, G., & Zamorani, C. 2002, *ApJ*, 565, L75
- [13] Fan, X., et al. 2000, *AJ*, 120, 1167
- [14] Fan, X., et al. 2001, *AJ*, 122, 2833
- [15] Feynmann, R. unpublished, as quoted in [16]
- [16] Fowler, W. A. 1964, *Rev. Mod. Phys.*, 36, 545, 1104E
- [17] Fryer, C. L., Woosley, S. E., & Heger, A. 2001, *ApJ*, 550, 372
- [18] Fuller, G. M., Woosley, S. E., & Weaver, T. A. 1986, *ApJ*, 307
- [19] Genzel, R., Eckart, A., Ott, T., & Eisenhauer, F. 1997, *MNRAS*, 291, 219
- [20] Ghez, A. M., Morris, M., Becklin, E. E., Tanner, A., & Kremenek, T. 2000, *Nature*, 407, 349
- [21] Gnedin, O. Y. 2001, *Class. & Quant. Grav.*, 18, 3983
- [22] Haehnelt, M. G., & Kauffmann, G. 2000, *MNRAS*, 318, L35
- [23] Ho, L. C. 1999, in *Observational Evidence for Black Holes in the Universe*, ed. S. K. Chakrabarti (Dordrecht: Kluwer), 157
- [24] Lai, D., Rasio, F. A., & Shapiro, S. L. 1993, *ApJS*, 88, 205
- [25] Loeb, A., & Rasio, F. A. 1994, *ApJ*, 432, 52
- [26] Macchetto, F. D. 1999, in *Towards a New Millennium in Galaxy Morphology*, ed. D. L. Block et al. (Dordrecht: Kluwer)
- [27] New, K. C. B., & Shapiro, S. L. 2001, *ApJ*, 548, 439
- [28] Rampp, M., Müller, E., & Ruffert, M. 1998, *A&A*, 332, 969
- [29] Rasio, F. A., & Shapiro, S. L. 1999, *Class. Quant. Grav.*, 16, 1
- [30] Rees, M. J. 1984, *ARA&A*, 22, 471
- [31] Rees, M. J. 1998, in *Black Holes and Relativistic Stars*, ed. R. M. Wald (Chicago: Chicago Univ. Press), 79
- [32] Rees, M. J. 2001, in *Black Holes in Binaries and Galactic Nuclei*, ed. L. Kaper, E. P. J. van den Heuvel, & P. A. Woudt (New York: Springer-Verlag), 351
- [33] Richstone, D., et al. 1998, *Science*, 395, A14
- [34] Saijo, M., Baumgarte, T. W., & Shapiro, S. L. 2003, submitted to *ApJ*, (astro-ph/0302436)
- [35] Saijo, M., Shibata, M., Baumgarte, T. W., & Shapiro, S. L. 2001, *ApJ*, 548, 919

- [36] Saijo, M., Shibata, M., Baumgarte, T. W., & Shapiro, S. L. 2002, *ApJ*, 569, 349
- [37] Schödel, R., et al. 2002, *Nature*, 419, 694
- [38] Shapiro, S. L. 2003, in *Carnegie Observatories Astrophysics Series, Vol 1: Coevolution of Black Holes and Galaxies*, ed. L. C. Ho (Cambridge: Cambridge Univ. Press), in press (astro-ph/0304202).
- [39] Shapiro, S. L. 2000, *ApJ*, 544, 397
- [40] Shapiro, S. L., & Shibata, M. 2002, *ApJ*, 577, 904
- [41] Shapiro, S. L., & Teukolsky, S. A. 1979, *ApJ*, 234, L177
- [42] Shapiro, S. L., & Teukolsky, S. A. 1983, *Black Holes, White Dwarfs, and Neutron Stars: The Physics of Compact Objects* (New York: Wiley Interscience)
- [43] Shibata, M., Baumgarte, T. W., & Shapiro, S. L. 2000a, *ApJ*, 542, 453
- [44] Shibata, M., Baumgarte, T. W., & Shapiro, S. L. 2000b, *Phys. Rev. D*, 61, 44012
- [45] Shibata, M., & Shapiro, S. L. 2002, *ApJ*, 527, L39
- [46] Soltan, A. 1982, *MNRAS*, 200, 115
- [47] Wagoner, R. V. 1969, *ARA&A*, 7, 553
- [48] Wilms, J., Reynolds, C. S., Begelman, M. C., Reeves, J., Molendi, S., Staubert, R., & Kendziorra, E. 2001, *MNRAS*, 328, L27
- [49] Yu, Q., & Tremaine, S., 2002, *MNRAS*, 335, 965
- [50] Zel'dovich, Ya. B., & Novikov, I. D. 1971, *Relativistic Astrophysics, Vol. 1* (Chicago: Univ. of Chicago Press)